Materials Chemistry and Physics 291 (2022) 126696

Contents lists available at ScienceDirect

Materials Chemistry and Physics

journal homepage: www.elsevier.com/locate/matchemphys

Synthesis and properties of electroless Ni–P-HfC nanocomposite coatings

Mohammad Farhan [1], Osama Fayyaz [1], Muddasir Nawaz, Ahmed Bahgat Radwan, R. A. Shakoor [*]

Center for Advanced Materials (CAM), Qatar University, 2713, Doha, Qatar

HIGHLIGHTS

- Incorporation of Hafnium carbide nanoparticles within the Ni–P matrix to develop nanocomposite coatings.
- Coating improving surface hardness upto 40% in comparison to pure Ni–P coating.
- Corrosion resistance improved upto 95% for Ni–P-0.75 g/L HfC nanocomposite coating in comparison to the steel substrate.
- Reduction in the active area caused by inert HfC leads to the improvement in corrosion resistance properties.

ARTICLE INFO

Keywords:
Nanocomposite coatings
Nanoparticles
Hardness
Electroless deposition
Corrosion
EIS

ABSTRACT

This work reports the development and characterization of Ni–P coatings with varying concentrations of hafnium carbide nanoparticles (HCNPs). Novel Ni–P-HCNPs nanocomposite coatings were developed on the A36 carbon steel by an electroless deposition technique. The effect of an increasing amount of HCNPs (0.25 g/L, 0.50 g/L, 0.75 g/L, and 1.00 g/L) on structural, compositional, microstructural, topographical, electrochemical and mechanical properties of Ni–P coatings was investigated. The structural (XRD, FE-SEM) and compositional analyses (EDX, XPS) confirm the successful incorporation of HCNPs into the Ni–P matrix. It is further noticed that the quantity of HCNPs has a substantial impact on modifying the microstructural, surface, mechanical, and corrosion resistance properties of Ni–P-HCNPs nanocomposite coatings. A comparative analysis of the properties of developed coatings suggests that nanocomposite coatings containing 0.75 g/L HCNPs demonstrate the highest improvement in hardness (~40%) and corrosion resistance (~95%) when compared to the Ni–P coatings. The increase in hardness can be attributed to the dispersion hardening effect experienced due to the presence of HCNPs. The improvement in the corrosion resistance properties can be ascribed to the reduction in the active sites of the Ni–P matrix and the filling of the micro pores with HCNPs. The attractive properties of HCNPs nanocomposite coatings provide an appealing option for their application in various industries such as aerospace, automobile, electronic, and oil & gas industry.

1. Introduction

The increasing demand for clean water and sufficient energy drives the rapid development of industries to fulfil these requirements. To overcome these challenges, new industries are established using more metallic components. Over time, metallic components tend to corrode due to severe operating conditions and harsh corrosive environments. This leads to a loss of performance and a decrease in efficiency, increasing the cost of operation. Therefore, protection from corrosion is essential for efficient utilization and prolonged component life. Surface modification of various categories is rigorously researched for the suitable and most appropriate corrosion mitigation strategies. Metallic coatings are a class of such strategies where a thin film is applied to protect the bulk material from corrosion and also provide better mechanical properties to enhance its life [1–3]. Nickel-based coatings are reported to possess better properties in terms of corrosion, and hardness values are even comparable to carcinogenic chromium coating, making them an exciting option for replacing the chromium coating. Among Nickel-based coatings, Nickel phosphorus coatings are well known for their effectiveness in marine corrosion and are reported to improve the

* Corresponding author.
E-mail address: shakoor@qu.edu.qa (R.A. Shakoor).
[1] Authors with equal contributions.

https://doi.org/10.1016/j.matchemphys.2022.126696
Received 9 June 2022; Received in revised form 26 July 2022; Accepted 20 August 2022
Available online 18 September 2022

mechanical properties of steel like abrasion, wear, and surface hardness [4,5]. Fabrication of Nickel phosphorus coatings through the electroless deposition method is considered to be most effective due to its high deposition rate, homogeneous deposition throughout the structure, better adhesion to the substrate, uniformity in layer thickness over the shapes, easier scalability, and economically feasible [6,7]. With the recent advancement in research and development, a novel method of reinforcing the binary alloy coating to enhance and ameliorate the properties of the nickel-phosphorus coating with the incorporation of hard ceramic particles to generate a class of composite coating is widely studied [8]. Incorporating micro/nanoparticles such as Al_2O_3, C_3N_4, ZrO_2, BN, SiC, TiN, SiO_2, B_4C TiC, WC, and TiO_2 [9–24] have led to the development of Ni–P based composite coatings with significant improvement in the properties like anti-corrosion, and wear resistance. Moreover, when the size of particles is in the nano range, interesting properties enhancement are noticed, like Si_3N_4 and CeO_2 enhancing the corrosion resistance of the Ni–P coatings [25,26]. In recent studies, problems like low toughness due to its hard nature and interdiffusion with the metal surface can be noticed with the accumulation of micro/nanoparticles in the Ni–P matrix [27]. On the other hand, metals in the form of micro/nanoparticles that have higher hardness, wear resistance, and moderate toughness, along with a better interface ability with the Ni–P matrix, can be used as reinforcement particles [28,29]. Hafnium (Hf) is a transition metal that has a very high melting point, low density, comprises of high strength, and demonstrates better corrosion resistance, almost unaffected by acids and alkalis. Hafnium Carbide (HfC) is considered the most refractory binary compound owing to its properties like relatively low vapour pressure, significantly high melting point (3890 °C), high phase stability, and low diffusion coefficient of oxygen [30–32]. Therefore, to further enhance the properties like hardness, toughness, and corrosion resistance of Ni–P coating, hard and inert HCNPs are reinforced in the Ni–P matrix to investigate the properties of Ni–P-HCNPs coatings that are not yet explored.

In this research, the Ni–P-HCNPs nanocomposite coatings were synthesized with an electroless deposition process by varying the concentrations of HCNPs to 0.25, 0.50, 075, and 1.00 g/L in the chemical bath. A36 carbon steel is selected as the substrate due to its application in the industries such as oil & gas, automotive, aerospace, and electronics [24]. A comparison in properties of pure Ni–P coating and synthesized Ni–P-HCNPs nanocomposite coatings is evaluated to examine the effect of HCNPs reinforcement on the structural, compositional, microstructural, mechanical properties, and corrosion resistance performance of the developed nanocomposite coatings.

2. Materials and methods

2.1. Preparation of substrates and coatings

A36 carbon steel (CS) alloy is utilized as the substrate to carry out the electroless deposition of Ni–P and Ni–P-HCNPs nanocomposite coatings. Firstly, the steel sheet is made into coupons of the dimension 30 × 30 × 2 mm^3, with the chemical composition presented in Table 1.

The substrate was sequentially polished using SiC abrasive sandpaper with various grit sizes (80, 120, 180, 220, 320, 500, 800, 1000, 1200, 1500, and 2000) to obtain smooth, mirror polished and flat surfaces. The coupons were cleaned with soap and tap water before changing to the next sandpaper. Sonication in acetone was carried out for 30 min to remove any loose particles or sand impurities adhered to the polished surface. It was then rinsed with distilled water before placing the coupons in the alkaline bath (3% NaOH +3% Na_2CO_3) for about half an hour at 60 °C. The coupons were then rinsed with DI water before acid pickling 15 wt% solutions of HCl for 45s. After the mentioned sequence of pretreatment procedures, the pretreated coupon is finally rinsed with DI water before placing it in the chemical bath to initiate an autocatalytic reaction leading to the deposition. The electroless deposition chemical bath was prepared with different concentrations of HCNPs of 0.25 g/L, 0.50 g/L, 0.75 g/L, and 1 g/L for Ni–P-HCNPs nanocomposite coatings to explore the influence of increased concentration. The chemical bath was designed by mixing Nichem 3010A and Nichem 3010B (Standard commercial-grade, Atotech Inc. Berlin, Germany) electroless deposition solution as presented in Table 2, along with optimized deposition conditions to obtain the best coatings.

2.2. Coatings process

The deposition process was carried out for a period of 120 min, and the temperature was maintained at 92 ± 2 °C, to prevent the sedimentation of the HfC nanoparticles during the deposition, the coating bath was stirred with the help of a magnetic stirrer at 350 rpm. Before initiating the deposition process, a respective concentration of HfC was mixed in 1L of chemical bath and agitated at the temperature of 92 ± 2 °C for 30 min to avoid any possibility of settling down and agglomeration of HCNPs. After the deposition process was completed, coated samples were removed from the coating bath and placed into the water bath at 60 °C for 10 min to gradually decrease the temperature of the substrate to avoid any kind of temperature-dependent deficiencies in the coating like cracking within the coating due to the sudden thermal stress as a result of lowering of temperature. The coated sample is then finally rinsed with deionized water, sonicated in acetone, and dried in air. With this perspective, all the coatings were categorized as, Ni–P, 0.25 g/L, 0.50 g/L, 0.75 g/L, and 1.00 g/L of HCNPs. For a better understanding of the Ni–P-HCNPs nanocomposite coatings, a schematic diagram of the electroless deposition system and the entire process is demonstrated in Fig. 1a and b.

2.3. Characterization of the coatings

The characterization and evaluation of the developed coating were done by using various characterization techniques. The XRD (X-ray diffraction) technique was used within the 2θ range of 20° to 100° at the 0.02° scanning rate for the structural and phase evaluation of the developed coatings. The surface morphology and elemental analysis of synthesized coatings of Ni–P and Ni–P-HCNPs were assessed by using a scanning electron microscope (SEM) and energy dispersive spectroscopy (EDX) from Nova Nano-450, ThermoFischer Scientific, Eindhoven, Netherland), respectively. An atomic force microscope (AFM) from Oxford Instruments, Goleta, CA, USA, was used to investigate topography and the heterogeneities of the developed coatings. A gauge meter

Table 2
Bath Constituents & Operating Conditions of the electroless coating bath.

Bath Constituents & Operating Conditions	Composition
Nichem 3010 A	57 ml/L
Nichem 3010 B	126 ml/L
Nanoscale HfC Particles	0.25–1.0 g/L
pH	4.2 ± 0.5
Temperature	92 ± 2 °C
Deposition time	120 min
Bath agitation	350 rpm

Table 1
The chemical composition of A36 carbon steel alloy.

Element	C	Cu	Mn	P	Si	S	Fe
Wt. %	0.29%	0.20%	1.03%	0.04%	0.28%	0.05%	Balance

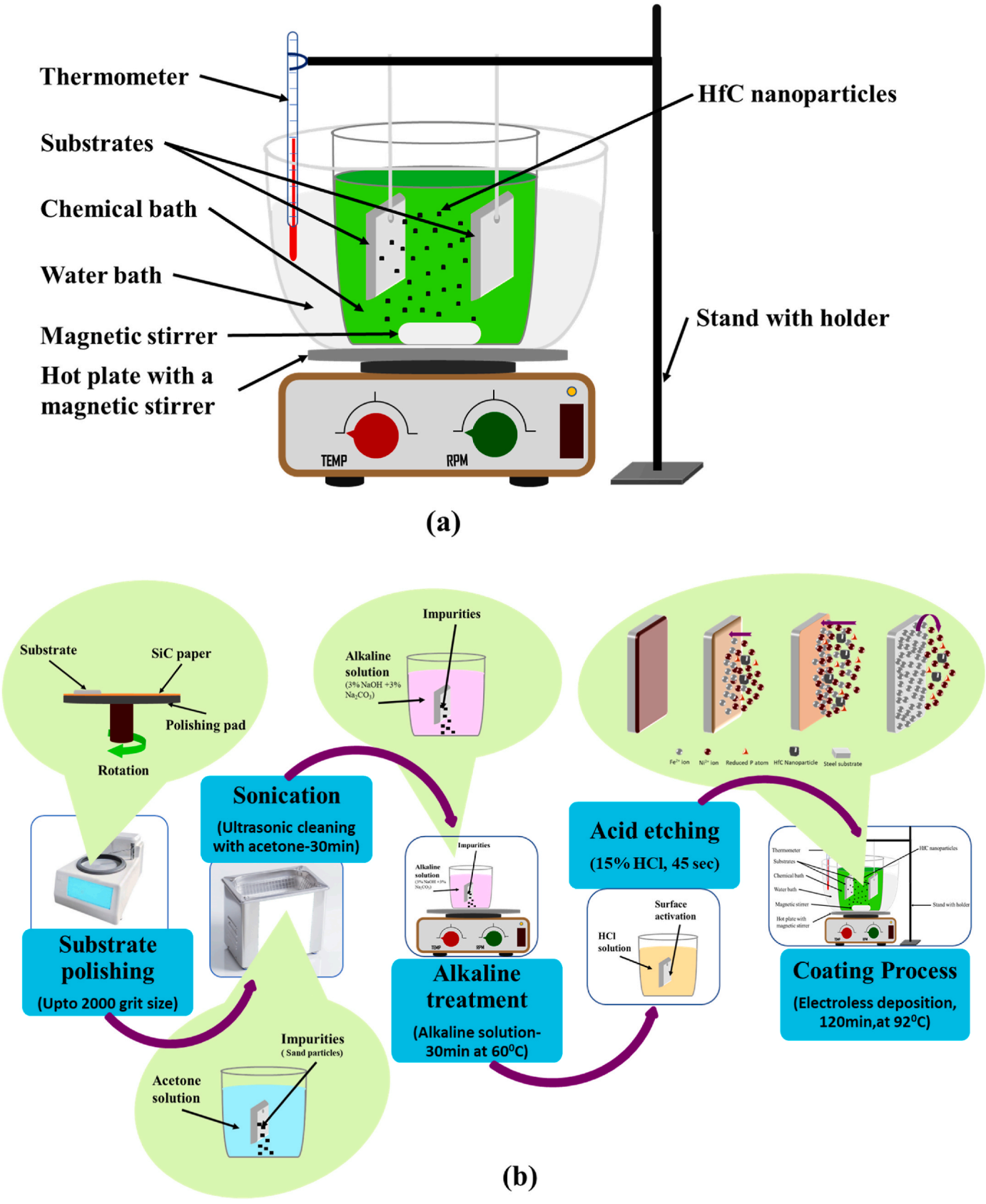

Fig. 1. A schematic diagram of the electroless deposition (a) system and (b) process.

(PosiTector 6000, DeFelsko, Proctor Avenue Ogdensburg, NY, USA), was utilized to determine the thickness of developed coatings. Microhardness and nanoindentation techniques have been applied to study the mechanical properties of the coatings. Vicker's microhardness tester (FM-ARS9000, USA), was used for the testing of microhardness, and the MFP-3D nanoindenter head fastened with AFM was used for nanoindentation measurement. The electrochemical impedance spectroscopy (EIS) technique was applied to analyze the corrosion behaviour of the developed coatings in 3.5 wt% NaCl solution with GAMRY 600 potentiostat/galvanostat/ZRA (Warminster, PA, USA). A three-electrode cell system was used where the coated sample was made as the working electrode, Ag/AgCl as the reference electrode and the graphite sheet as the counter electrode. Moreover, perturbation of 10 mV was provided for the frequency range of 10^{-2}-10^{5} Hz for the EIS measurement, while ±0.25V of the range was selected from open circuit potential (OCP) with a step of 0.167 mV for generating potentiodynamic polarization data set [6,10,24,37].

3. Results and discussion

3.1. Structural and compositional analysis

3.1.1. XRD analysis

The XRD technique was applied to investigate the structure and phase of the developed nanocomposite coatings. The XRD pattern of Ni–P and different compositions of Ni–P-HCNPs nanocomposite coating are presented in Fig. 2. All the coatings showed a broad peak at 2θ, varying from 40° to 50°, which attributes to the creation of a semi-amorphous structure. The broad peak at 2θ ~44.6° is due to the Ni–P coating. Moreover, new peaks were observed after the successful incorporation of the HCNPs into the Ni–P matrix. Peaks at 2θ ~33.3°, 38.8°, 56°, and 66.8° represents Ni (011), HfC (111), HfC (002), HfC (022), and HfC (113) plane for the face-centered cubic (FCC) structure, respectively (ref. Code ICDD: 98-061-8010). The intensity of HfC peaks increases with the increment in the reinforcement concentration, which suggests the efficient incorporation of HCNPs in the Ni–P matrix. The presence of phosphorous atoms in the nickel crystalline structure causes the lattice distortion that provides a hindrance to the propagation of nickel atoms to occupy face-centered cubic, which leads to the formation of an amorphous structure. The formation of an amorphous structure was also reported in previous literature [33–35].

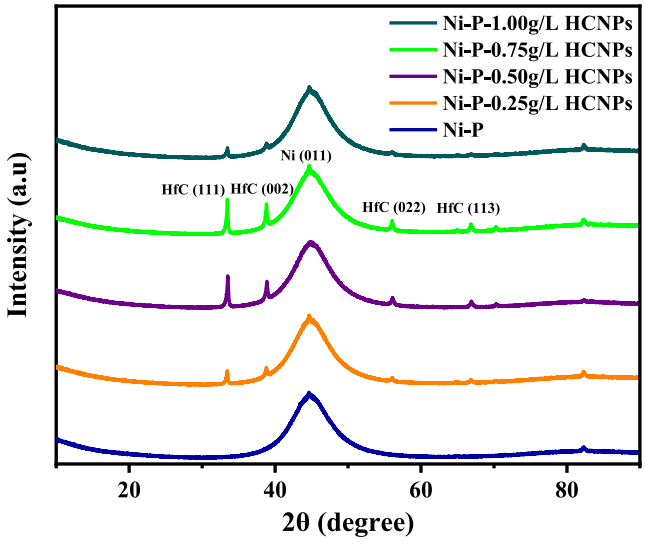

Fig. 2. XRD pattern of Ni–P and Ni–P-HCNPs with different concentrations of HCNPs nanocomposite coatings.

3.1.2. X-ray photoelectron spectroscopic analysis

XPS survey spectra of Ni–P-0.75 g/L HCNPs nanocomposite coating are displayed in Fig. 3, and respective elements of the coatings are marked based on their position over the axis of binding energy. Peaks of Ni2p, P2p, Hf4f, and C1s can be clearly observed, indicating their presence in the nanocomposite coating. Peak representing oxygen could be due to the formation of superficial oxides or impurities prior to the installation of the sample for analysis.

Highly magnified spectra of each element with their respective chemical state are presented in Fig. 4. Lorentzian-gaussian fit over the experimental data was carried out, and a Tougaard background correction was employed to obtain the deconvoluted peaks of the elements in their actual chemical state. Fig. 4a shows the photoionization spectra of Ni2p that lie in the binding energy range of 845 eV–882 eV. Deconvoluted peaks positioned at 852.3 eV and 869.5 eV indicate Ni2p3/2 and Ni2p1/2 of nickel in its metallic form alongside their satellite peaks around 860 eV and 877.5 eV. However, peaks shown at 853.9eV and 872eV can be recognized as the oxides and/or hydroxides of nickel for the Ni2+ chemical state, respectively [36–38]. Fig. 4b expresses the peaks of phosphorus (P2p) in its deconvoluted form, peaks of P2p3/2 and P2p1/2 can be identified at 129. eV and 129.9 eV indicate the elemental form of phosphorus. Moreover, a peak located at 131.5 eV can be allotted to hypophosphites or phosphorus in its intermediate chemical states that might have been left as the solid solution in nanocomposite coatings [36–39]. Fig. 4c depicts deconvoluted peaks of Hf4f, confirming the presence of hafnium carbide phase with the shifted peak of metallic hafnium around 13.7 eV, carbide peak can further be identified at 17.5 eV revealing and confirming the Hf–C bond [40–42]. The absence of any other oxidation state of Hf4f can be accepted as the inactive and inert nature of reinforcement toward the reactions occurring in the chemical bath during the entire electrodeposition process. Furthermore, Fig. 4d shows the deconvolution diagram of C1s, the peak observed at 283.2eV can be ascribed to C–Hf for the hafnium carbide along with the C–C and C═O peaks located around 284.8 eV and 287.3 eV attributing to the environmental impurities of adventitious carbon in its various state as reported in the literature [40,43–45].

3.2. Surface morphology of Ni–P and HCNPs coatings

The results of SEM assessment of Ni–P and different compositions of Ni–P-HCNPs nanocomposite coatings for the surface morphology are specified in Fig. 5a–e For a clear demonstration of the effect of introducing and increasing the integration of HCNPs in the Ni–P matrix. Ni–P coatings show a colony-like well-defined columnar microstructure with

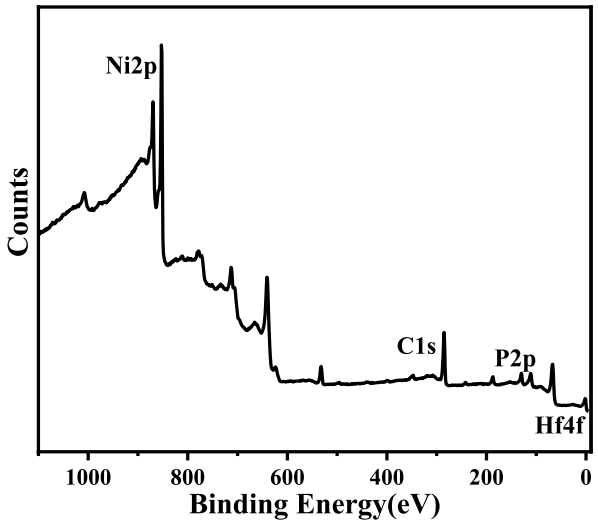

Fig. 3. Survey spectra of Ni–P-0.75 g/L HCNPs nanocomposite coating.

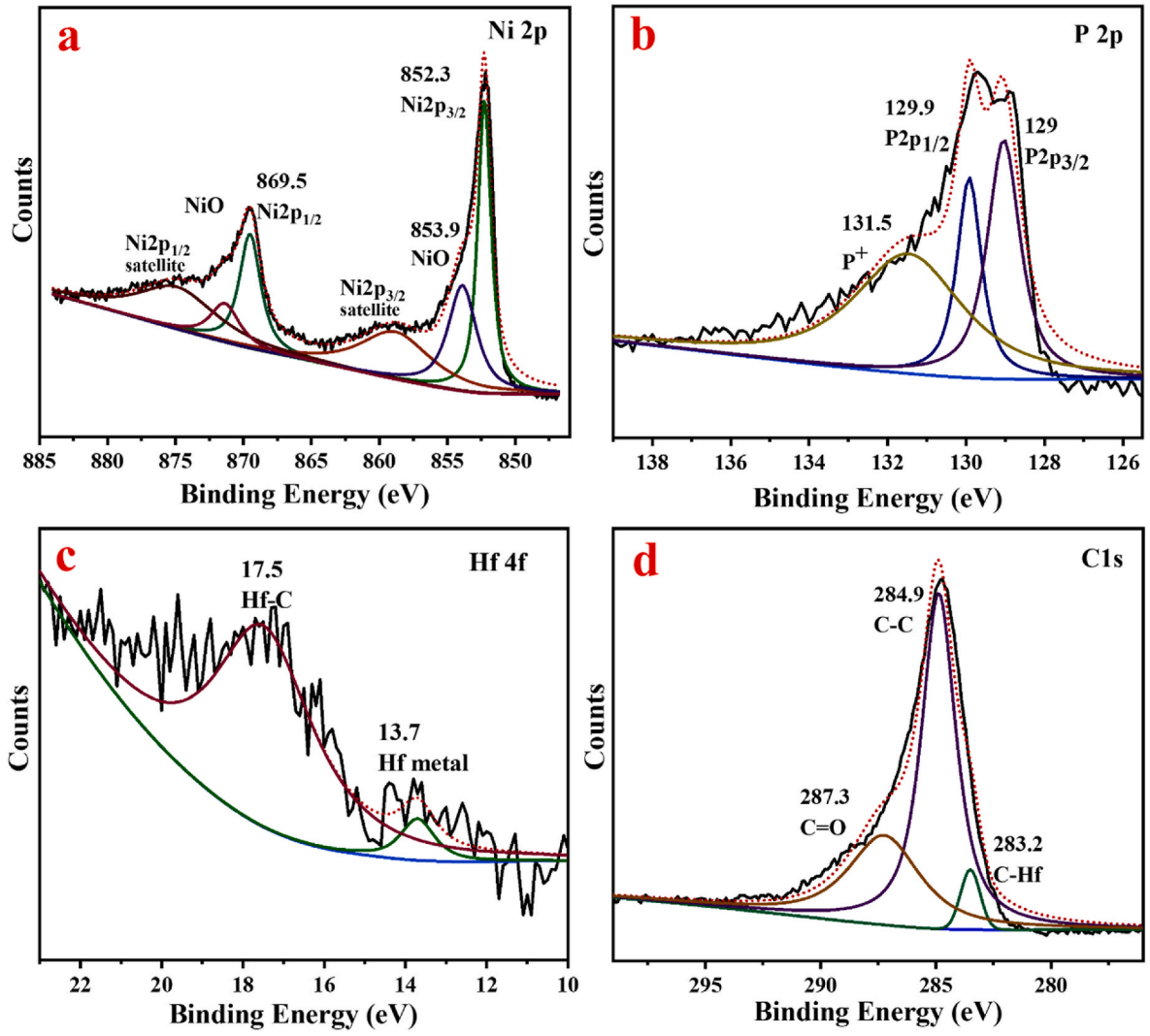

Fig. 4. XPS spectra of Ni–P-0.75 g/L HCNPs (a) Ni2p, (b) P2p, (c) Hf4f and (d) C1s.

partial irregular globules and visible micropores, revealing the reported deficiency of pure Ni–P coating possessing micropores throughout the film [1,46,47,50]. Introducing the Hafnium carbide to the chemical bath has completely transformed the columnar microstructure of Ni–P coating to the planar morphology of Ni–P-0.25 g/L HCNPs. Furthermore, increasing the HCNPs concentration in the chemical bath seems to increase the nodules with decreasing nodular size, indicating that HCNPs are behaving as heterogeneous nucleation sites for nickel and phosphorus ions to be deposited. These reinforcements further lead to the development of grain growth after it is deposited over the substrate. The large surface area of nanoparticles provides this nodular growth and size of the nodule. Moreover, after the concentration of HCNPs is increased in the chemical bath, excessive nucleation sites are created, and the size of the nodule decrease due to an increased number of nodular formation at the substrate, as observed in Fig. 5b-d. However, when the terminal value of nano-reinforcements is achieved, particle agglomeration adversely affects the formation of nanocomposite coating, reverting to columnar structure with a significant number of micropores as seen in Fig. 5 e for 1.0 g/L [48]. The elemental mapping micrograph of the 0.75 g/L of HCNPs is presented in Fig. 5(d_1-d_4). The presence and uniform dispersion of respective elements of nickel, phosphorus, and hafnium are clearly evident, ascribing to the formation of a high-quality nanocomposite coating.

Fig. 6a–e presents the EDX scan spectra of (a) Ni–P, (b) 0.25, (c) 0.50, (d) 0.75, and (e) 1.00 g/L of HCNPs nanocomposite coatings, and the element mappings are shown as an inset, respectively. EDX mapping technique was applied to examine the influence of HCNPs on the Ni–P matrix and the chemical compositions of the nanocomposite coatings. In Fig. 6b-e, the presence of hafnium (Hf) peaks in the EDX spectra indicates the successful incorporation of HCNPs into the surface and subsurface layers of the developed coatings along with the nickel (Ni) and phosphorus (P). The weight percentage of Ni–P coatings contains nickel of about 88.21%, and the rest was balanced by phosphorus atoms. A gradual increase in the concentration of Hf is observed from 0.54 wt% to 5.82 wt% for the concentrations of HCNPs from 0.25 to 0.75 g/L, and then a slight decrease is observed for the 1.00 g/L concentration of 3.42% wt.%.

The various weight percentage of elements presented in the developed nanocomposite coating that was obtained through the EDX findings are tabulated in Table 3. The results provided by the EDX assessment confirm the successful integration of HCNPs in the composite coatings, which shows the compositions present in coatings depend on the concentration present in the chemical bath [49]. Moreover, the concentration of nickel is seen to decrease, which is replaced by HCNPs, keeping the concentration of phosphorus nearly the same, indicating the replacement of nickel in the formation of coating as mid-concentration of phosphorus (8%–12%) is reported to possess the superior corrosion resistance with adequate mechanical properties. A decrease in the concentration of HCNPs for 1.00 g/L can be due to non-uniform agglomerated HCNPs in the coating in certain regions. The addition of HCNPs

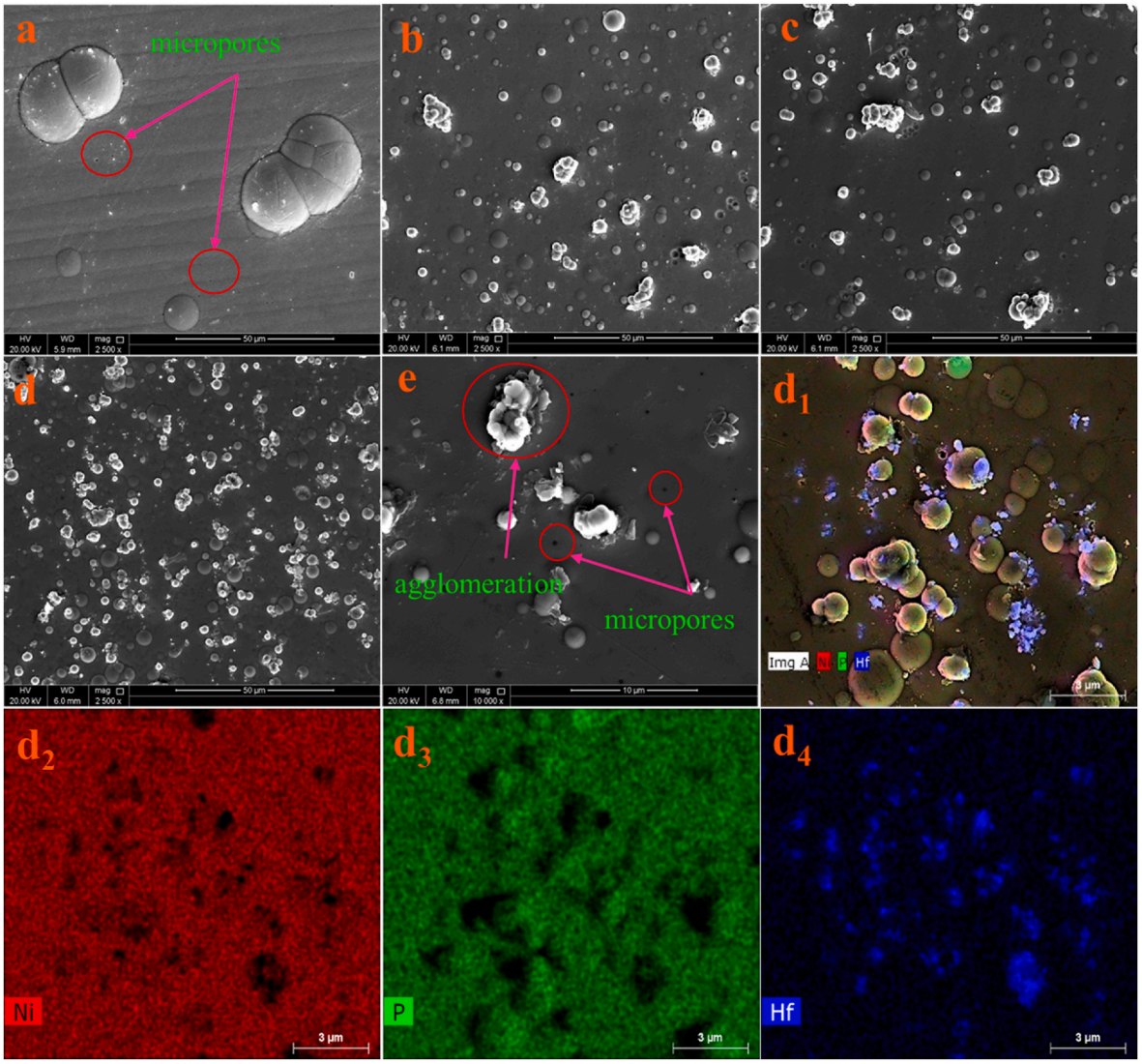

Fig. 5. Scanning electron microscope (SEM) image of the (a) Ni–P, (b) 0.25, (c) 0.50, (d) 0.75, (e) 1.00 and (d_1-d_4) Ni–P-0.75 g/L of HCNPs in the developed nanocomposite coating.

and increase in the concentration of HCNPs decreases the wt.% of nickel but has no significant effect on wt.% of phosphorus which remains around 11% for all compositions of coatings. These results are in agreement with the previous literature [50].

3.3. The atomic force microscope (AFM) technique

The AFM technique was used for the evaluation of the surfaces for developed nanocomposite coatings. The three-dimensional topographic images of (a) Ni–P, (b) 0.25, (c) 0.50, (d) 0.75, and (e) 1.00 g/L of HCNPs nanocomposite coatings are presented in Fig. 7a–e. From the images, it can be noticed that Ni–P coating has a smoother surface than the other Ni–P-HCNPs composition coatings. To have a better grasp of the impact of HCNPs on the surface of developed composite coatings, a comparison is presented in Table 4. The quantitative analysis results show an increasing trend in average surface roughness (Ra) from 7.68 nm to 25.02 nm with an increase in the concentration of the HCNPs from 0 to 1.00 g/L, leading to three times surface roughness improvement. Also, a similar trend can be seen for root mean square surface roughness (Rm) from 10.40 nm to 31.73 nm for the composition of Ni–P to Ni–P-1.00 g/L HCNPs in Table 4. Furthermore, coating surfaces of Ni–P, 0.25, 0.50, and 0.75 g/L of HCNPs, have asperities and peaks. However, a canyon-like structure can be seen on the surface of the Ni–P-1.00 g/L HCNPs composite coating. The previous literature validates the increase in surface roughness due to the incorporation of nanoparticles in the Ni–P matrix [36,51]. The increasing amount of hard and insoluble HCNPs can be ascribed to the increase in surface roughness which can obstruct and create a barrier in the path of the AFM cantilever probe tip for its smooth movement on the coating surfaces.

3.4. Mechanical properties

The results of microhardness of the Ni–P and Ni–P-HCNPs with the concentration (0.25, 0.50, 0.75, and 1.00 g/L of HCNPs) nanocomposite coatings are 506 HV, 579 HV, 629 HV, 700 HV, and 663 HV, respectively, are shown in Fig. 8. The increasing trend of microhardness with the increment in the concentrations of HfC nanoparticles up to a certain quantity can be observed. The highest values of microhardness (700 HV_{50}) are achieved for the Ni–P-0.75 g/L HCNPs composition, which is ~40% more in comparison to Ni–P coatings. An improvement in hardness can be considered as the influence of the grain refinement strengthening and dispersion hardening increased due to the incorporation of HCNPs in the Ni–P matrix. The presence of hard ceramic HCNPs provides a barrier to the movement of dislocation during the

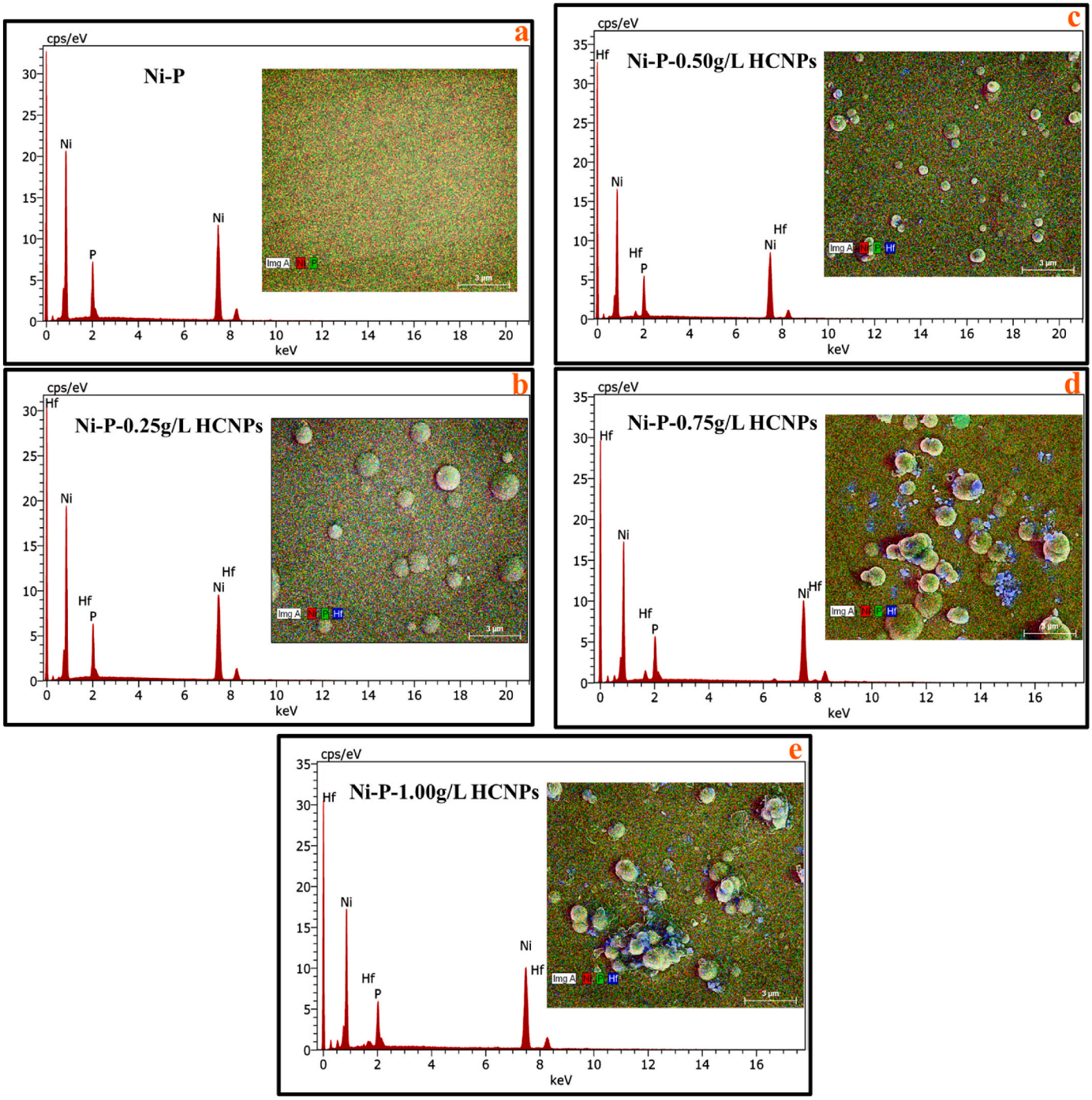

Fig. 6. The energy dispersive spectroscopy (EDX) scan spectra along with elemental mapping of (a) Ni–P, (b) 0.25, (c) 0.50, (d) 0.75, and (e) 1.00 g/L of HCNPs nanocomposite coatings.

Table 3
Quantitative evaluation of the various elements obtained in the nanocomposite coatings through EDX scan.

Coating composition	Nickel (wt.%)	Phosphorus (wt.%)	Hafnium (wt.%)
Ni–P	88.21%	11.79%	–
Ni–P-0.25 g/L HCNPs	87.85%	11.62%	0.54%
Ni–P-0.50 g/L HCNPs	85.92%	11.05%	3.03%
Ni–P-0.75 g/L HCNPs	84.23%	9.95%	5.82%
Ni–P-1.00 g/L HCNPs	85.79%	10.79%	3.42%

mechanical deformation process and thus impedes the movement of the dislocation. During the deformation, HCNPs act as an obstacle that does not deform. Because of that, the moving dislocations have to change their path and bypass the obstacles due to the dispersion hardening process, whereas the dislocation motion is also obstructed at the grain boundaries because of the material strengthening provided by the grain refinement process [52]. Reduction in lateral grain growth and creation of a fine structure occurs due to the acceleration of nucleation rate, because of the presence of various heterogeneous nucleation sites, with the uniform dispersion of HCNPs into the coating. The incorporation of HCNPs into the Ni–P matrix and the filling of the pores also led to microhardness improvement and enhanced the load-bearing ability

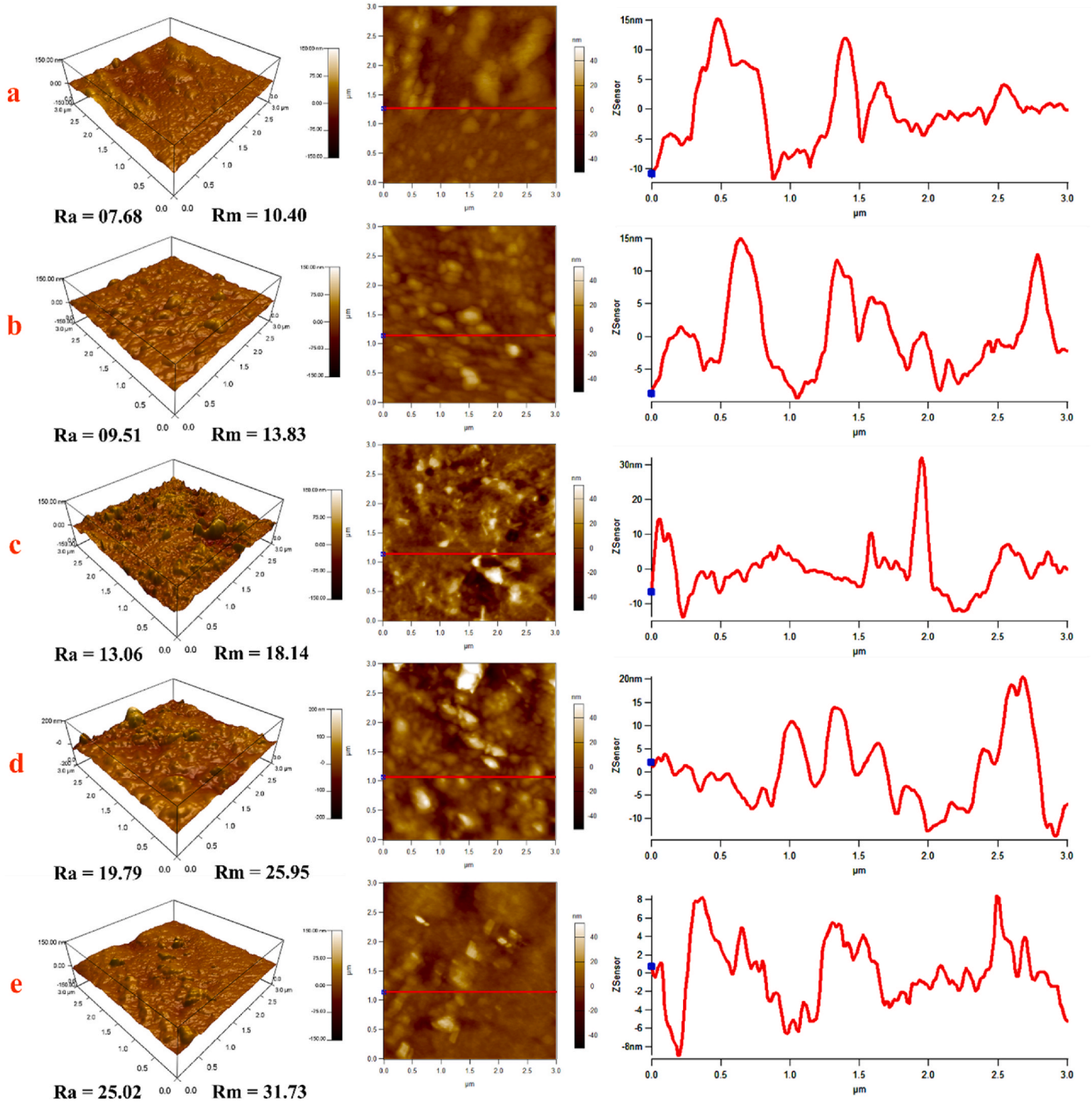

Fig. 7. The AFM micrograph with the 3D topographic profile of the surface roughness of (a) Ni–P, (b) 0.25, (c) 0.50, (d) 0.75, and (e) 1.00 g/L of HCNPs nanocomposite coatings.

[53].

With an additional increase in the concentration of HCNPs, the hardness decreases to 663 HV_{50} at Ni–P-1.00 g/L HCNPs composition after reaching its highest value. It could be depicted owing to the over-concentration of HCNPs into the Ni–P matrix, which reduces the properties like microhardness and load-bearing. These results consistency also noticed in previous literature [54]. The nanoindentation test has been used to investigate the mechanical properties of the Ni–P and Ni–P-HCNPs nanocomposite coatings at the nanoscale. A Berkovich diamond indenter tip (nanoindenter head) is attached to the AFM for the nanoindentation test by applying 1 mN force at a scanning rate of 200 μN/s with a dwell time of 10s for the loading and unloading process. The loading and unloading curves of nanocomposite coating with different concentrations of HfC are presented in Fig. 9. Maximum indentation depth of Ni–P coating gradually decreases from 257.01 nm to 230.49 nm because of the dispersion hardening effect leading to microhardness improvement and enhancing the load-bearing ability because of the incorporation of HCNPs in the Ni–P matrix as previously explained. It can also be observed an increase in indentation depth of ~10 nm at the Ni–P-1.00 g/L HCNPs composition, and it is because of over-concentration of nanoparticles accumulated in the Ni–P matrix, thus having an adverse effect on mechanical properties, that were noticed in previous studies [36,43,55]. The lowest indentation depth was noticed at the composition of Ni–P-0.75 g/L HCNPs because of the

Table 4
Comparison of roughness for Ni–P, 0.25, 0.50, 0.75, and 1.00 g/L of HCNPs nanocomposite coatings.

Parameters Measured Values					
Composition	Ni–P	Ni–P-0.25 g/L HCNPs	Ni–P-0.50 g/L HCNPs	Ni–P-0.75 g/L HCNPs	Ni–P-1.00 g/L HCNPs
Average Roughness (R_a), nm	7.68	9.51	13.06	19.79	25.02
Root Mean Square Roughness (R_m), nm	10.40	13.83	18.14	25.95	31.73

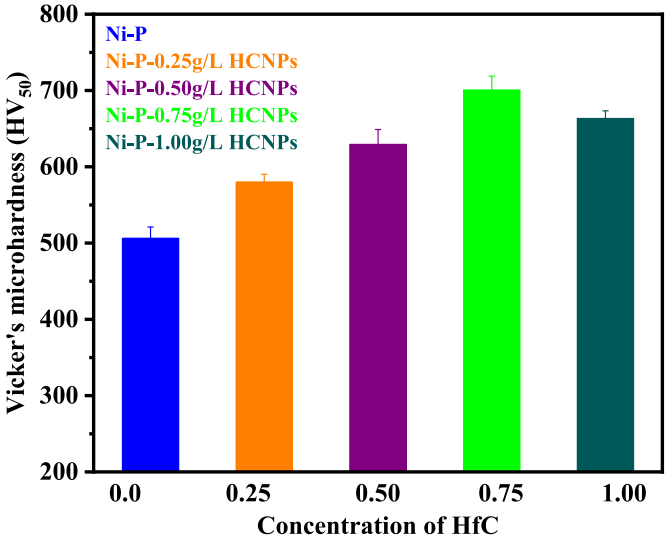

Fig. 8. Vickers microhardness (HV_{50}) results for Ni–P, 0.25, 0.50, 0.75, and 1.00 g/L of HCNPs nanocomposite coatings.

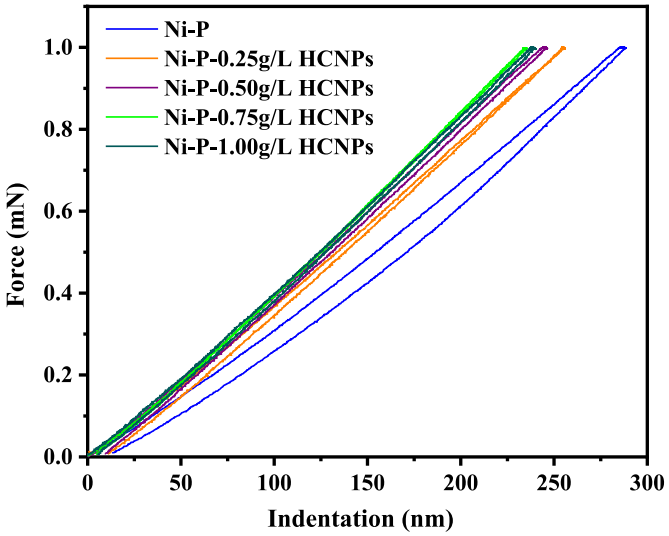

Fig. 9. Nanoindentation curve for Ni–P, 0.25, 0.50, 0.75, and 1.00 g/L of HCNPs nanocomposite coatings.

uniform thickness and proper distribution of HCNPs into the matrix with no agglomeration in the composite coating. The uniformity of loading and unloading curves with no kinks suggests that the crack-free and pore-free nanocomposite coatings were synthesized. Furthermore, the hardness increased from 5.06 GPa to 7.10 GPa, along with elastic modulus (E_c), from 8.41 GPa to 10.48 GPa with an increase in concentration from 0.25 g/L to 0.75 g/L, and then decreased at 1 g/L of HfC particles in the nanocomposite coatings which supports the findings of previous studies that the incorporation of nanoparticles increases the hardness of Ni–P matrix [56]. The agglomeration that occurs at the composition of Ni–P-1.00 g/L HCNPs is responsible for the decrease in hardness which aligns with the findings of Vickers microhardness testing. The formation of composite structure, grain refinement, and dispersion hardening lead to the increase in elastic modulus and hardness of the composite coatings [54,56]. A quantitative assessment of the indentation findings in response to mechanical properties is comprised in Table 5.

3.5. Corrosion resistance behaviour

The corrosion performance of the electroless deposited Ni–P-HCNPs nanocomposite coatings with various concentrations of HCNPs through electrochemical impedance spectroscopy (EIS) and potentiodynamic polarization (PP) technique, the corrosion test was performed in 3.5 wt % of NaCl solutions at 25 °C.

3.5.1. Electrochemical impedance spectroscopy (EIS) measurements

The corrosion resistance of electroless deposited Ni–P coatings with various concentrations of HCNPs was analyzed by the EIS method at normal room temperature. Bode plots of the carbon steel, Ni–P, and various compositions of Ni–P-HCNPs are shown in Fig. 10a and b. Before starting the electrochemical measurements, the coated substrate with an exposed area of 2.86 cm^2 was placed into 3.5 wt% of NaCl solution at OCP for 60 min to stabilize. Based on a modified Randle, an equivalent circuit and cascaded double time constant circuit was used for the fitting of the obtained data, as shown in Fig. 10a and b. The various EIS parameters of nanocomposite coatings, such as the solution resistance (R_s), pore resistance (R_p), charge transfer resistance (R_{ct}), and constant phase elements CPE_1 and CPE_2 were obtained from measured data after curve fitting. To account for the surface inhomogeneity, equation (1) is used to calculate the CPE_1 and CPE_2 (constant phase elements) instead of capacitors for the coated substrate from the data obtained through electrochemical impedance spectroscopy (EIS) plots [57] (see Fig. 12).

$$\frac{1}{ZCPE} = Q(j\omega)^n \tag{1}$$

where the Q is admittance (CPE constant), ω the angular frequency of the AC signal, j is the imaginary number, and n is the exponent of CPE, when n is equal to 1 element, becomes a pure capacitor, n *is* equal to zero is for the pure resistor, and $0 < n < 1$ represents the deviation from the ideal behaviour.

The bode plot for carbon steel in the medium–high-frequency regions indicate the one-time constant, while the two-time constant for the coated substrate is demonstrated by the broadening of the phase angle. After the curve fitting for analyzed data through an equivalent circuit,

Table 5
Nanoindentation results of Ni–P, 0.25, 0.50, 0.75, and 1.00 g/L of HCNPs nanocomposite coatings.

Characteristic	Ni–P	Ni–P-0.25 g/L HCNPs	Ni–P-0.50 g/L HCNPs	Ni–P-0.57 g/L HCNPs	Ni–P-1.00 g/L HCNPs
Elastic Modulus-E_c (GPa)	8.41	8.83	9.61	10.48	10.01
Maximum Indentation-Depth H_{max} (nm)	257.01	252.06	246.50	230.49	240.21
Final Indentation Depth H_c (nm)	92.67	85.30	79.98	73.90	77.29
Hardness (GPa)	5.06	5.61	6.39	7.10	6.63

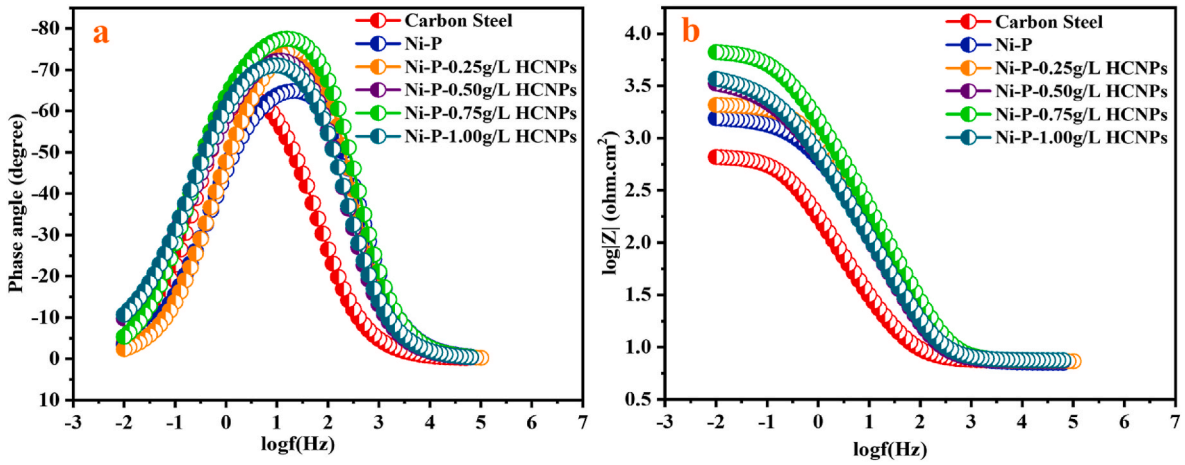

Fig. 10. Bode plots **(a)** Phase angle – Frequency and **(b)** Impedance – Frequency of CS, Ni–P, 0.25, 0.50, 0.75, and 1.00 g/L of HCNPs nanocomposite coatings.

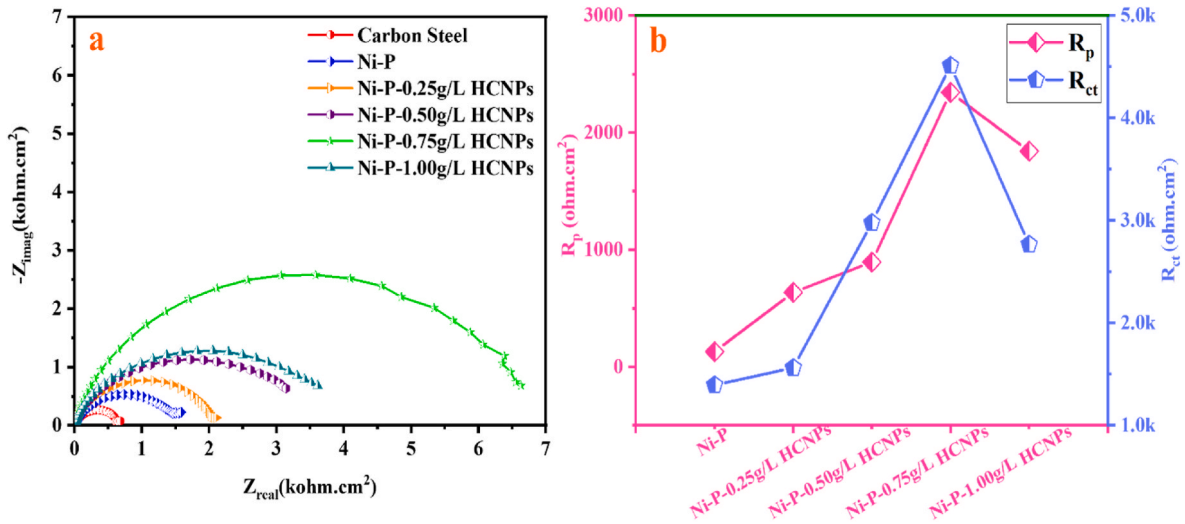

Fig. 11. (a) Nyquist plot, and (b) R_p and R_{ct} curve with the HCNPs concentrations of CS, Ni–P, 0.25, 0.5, 0.75, and 1.00 g/L of HCNPs nanocomposite coatings.

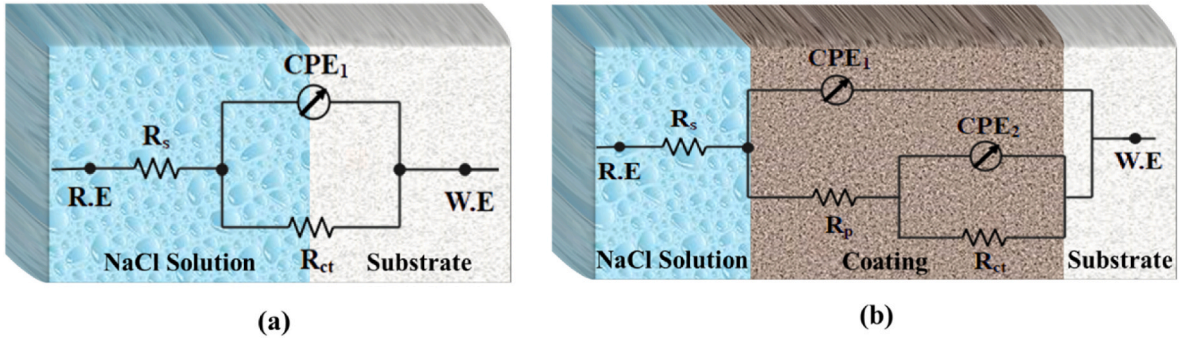

Fig. 12. (a) One-time constant, (b) two–time constants, equivalent electric circuits to EIS fit for CS, Ni–P, 0.25, 0.50, 0.75, and 1.00 g/L of HCNPs nanocomposite coatings.

the magnitude plot of carbon steel shows the lowest corrosion resistance value of ~560 Ω cm^2. In the case of Ni–P coating, impedance magnitude reaches ~1490 Ω cm^2. This improvement in corrosion resistance is attributed to the creation of the hypophosphite layer, as reported in the literature [11,24,37]. The integration of HCNPs in the Ni–P matrix further broadens the phase angle, which leads to the improvement in the impedance response values of nanocomposite coatings. The reduction of active corrosion sites because of hard, inert, and non-corrosive HCNPs contributes to the increase in the impedance value for nanocomposite coatings. The impedance value of the Ni–P-0.75 g/L HCNPs composite coating was observed to be almost four times of the Ni–P composite coating (Fig. 10a). Successive increase in HCNPs concentration from 0.25 g/L to 0.75 g/L has led to an efficient improvement in corrosion resistance with the highest value of impedance at Ni–P-0.75 g/L HCNPs

Table 6
Electrochemical impedance spectroscopy (EIS) fitting results of the CS, Ni–P, and 0.25, 0.50, 0.75, 1 g/L HCNPs nanocomposite coatings that immersed in 3.5 wt % NaCl solution at 25 °C.

Sample	R_{ct} (Ωcm^2)	R_{po} (Ωcm^2)	Corrosion protection efficiency (PE%)
Carbon Steel	556	–	–
Ni–P	1283	300	56.7
Ni–P-0.25 g/L HfC	1648	500	66.3
Ni–P-0.50 g/L HfC	2966	900	81.3
Ni–P-0.75 g/L HfC	5495	1500	94.5
Ni–P-1.00 g/L HfC	3153	1300	82.4

composition with 6.4 kΩ cm^2 (see Table 6). The occupancy of HCNPs in the micropores of the Ni–P matrix reduces the conductive path and thus increases pore resistance [58]. The hindrance created between the electrolyte path reaching the substrate because of the increasing HCNPs concentration in the Ni–P matrix minimizes the active area for the corrosion initiation. The various distinct capacitive loops of carbon steel, Ni–P, and Ni–P-HCNPs composite coating are displayed in the Nyquist plot as seen in Fig. 10a, revealing a similar trend as indicated by the Bode plot. The pore resistance increased because of the successful integration of HCNPs in the Ni–P matrix, which hindered electrolyte attack on the substrate by reducing the active sites leading to an improvement in Rct as presented in Fig. 9b. Furthermore, corrosion resistance of coatings increases with the decrease in active sites by increasing the concentration of HCNPs in the coating bath.

3.5.2. Potentiodynamic polarization measurements

The potentiodynamic polarization method was adopted to evaluate the corrosion behavior of the coating within the range of −0.25 to 0.25 V from open circuit potential with a scan rate of 0.167 mV.s-1 for the carbon steel, Ni–P, and Ni–P-HCNPs with different concentrations of HCNPs in the composite coatings. The Tafel plots of the carbon steel, Ni–P, 0.25, 0.50, 0.75, and 1.00 g/L of HCNPs nanocomposite coatings are shown in Fig. 13. Electrochemical parameters of the various coatings, i_{corr} (corrosion-current density), E_{corr} (corrosion-potential), β_a (anodic Tafel slopes), β_c (cathodic Tafel slopes), R_P (polarization resistance), and corrosion protection efficiency (PE%) are calculated by Tafel

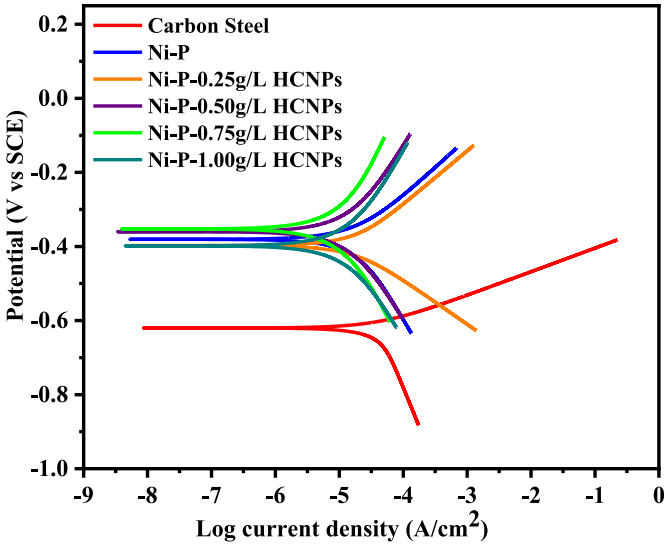

Fig. 13. Tafel curves for CS, Ni–P, 0.25, 0.50, 0.75, and 1.00 g/L of HCNPs nanocomposite coatings.

Table 7
Tafel fitting results of the CS, Ni–P, 0.25, 0.50, 0.75, and 1.00 g/L of HCNPs nanocomposite coatings immersed in 3.5 wt % NaCl solution at 25 °C.

Sample	E_{corr} (V)	i_{corr} (μA/cm^2)	$-\beta_c$ (V/decade)	β_a (V/decade)	R_P (Ωcm^2)	(PE %)
Carbon Steel	−0.620	39.719	−0.173	0.104	710	–
Ni–P	−0.381	19.498	−0.185	0.154	1839	50.91
Ni–P-0.25 g/L HCNPs	−0.397	16.481	−0.181	0.242	2678	58.50
Ni–P-0.50 g/L HCNPs	−0.359	12.387	−0.267	0.255	4566	68.81
Ni–P-0.75 g/L HCNPs	−0.352	8.440	−0.313	0.337	8310	78.75
Ni–P-1.00 g/L HCNPs	−0.398	12.105	−0.263	0.290	4929	69.50

extrapolation technique as shown in Table 7.

The following equations (2) and (3) are used to calculate the corrosion protection efficiency and polarization resistance of the coatings from the data acquired through Tafel plots [57,59].

$$PE\% = 1 - \frac{i_{corr2}}{i_{corr1}} \times 100\% \quad (2)$$

$$R_P = \frac{\beta_a|\beta_c|}{2.303(\beta_a + |\beta_c|)icorr} \quad (3)$$

where the i_{corr1} and i_{corr2} are corrosion current densities for the carbon steel and nanocomposite coatings, respectively.

For carbon steel, the highest value of 39.719 μA/cm^2 current density was observed with a corrosion potential of −0.620 V, considered most prone to corrosion, as shown in Fig. 11. The Ni–P has a current density of 19.498 μA/cm^2 which further decreased with increasing the HCNPs concentration in the composition of Ni–P-0.25 g/L HCNPs (16.481 μA/cm^2), Ni–P-0.50 g/L HCNPs (12.387 μA/cm^2), Ni–P-0.75 g/L HCNPs (8.440 μA/cm^2), and Ni–P-1g/L HCNPs (12.105 μA/cm^2) into the Ni–P matrix. Furthermore, the corrosion potential of Ni–P coating shows a slightly more anodic and increases from −0.381 V to −0.352 V with an increment in the concentration of HCNPs, which indicates slightly more inhibition of the anodic activities in the Ni–P matrix. This trend indicates that the presence of HCNPs in the coating reduces the anodic activities. The presence of HCNPs reduces the active sites for the chloride ion absorption on the surfaces with pores and.

Cracks. Overall, the increase in reinforcement concentration leads to the improvement in corrosion resistance in favour of previous studies [60].

4. Conclusions

Ni–P coatings containing varying concentrations of hafnium carbide nanoparticles (HCNPs) were developed through an electroless coating process and characterized. It is observed that the amount of HCNPs has a significant effect on modifying the microstructural surface properties. Which increases the mechanical and corrosion resistance properties of Ni–P-HCNPs nanocomposite coatings due to efficient blocking of the micropores and dispersion hardening effect. The developed novel Ni–P-HCNPs nanocomposite coatings reveal their best performance at the concentration of 0.75 g/L, showing an improvement in hardness (~40%) and corrosion resistance (~95%) when compared to the Ni–P coatings. The tempting properties of Ni–P-HCNPs nanocomposite coatings make them attractive for oil and gas, automobile, aerospace, and many other related industries.

CRediT authorship contribution statement

Mohammad Farhan: Methodology, Formal analysis, Investigation, Writing – original draft. **Osama Fayyaz:** Methodology, Conceptualization, Validation, Writing – review & editing. **Muddasir Nawaz:** Writing – review & editing, Validation, Resources. **Ahmed Bahgat Radwan:** Resources, Formal analysis. **R.A. Shakoor:** Supervision, Writing – review & editing, Project administration, Funding acquisition.

Declaration of competing interest

The authors declare that they have no known competing financial interests or personal relationships that could have appeared to influence the work reported in this paper.

Data availability

The data that has been used is confidential.

Acknowledgment

The present work is supported by Qatar University Grants (IRCC-2020-006 and IRCC-2022-491). The opinions expressed in this article are solely the responsibility of the authors. The authors acknowledge the services of the Central Laboratory Unit (CLU), Qatar University for Microstructural analysis (FE-SEM/EDS). XPS facility of Gas Processing Center (GPC), Qatar University, was utilized to study compositional analysis. Open Access Funding is provided by the Qatar National Library (QNL)

References

[1] J. Li, H. Zeng, J.L. Luo, Probing the corrosion resistance of a smart electroless Ni-P composite coating embedded with pH-responsive corrosion inhibitor-loaded nanocapsules, Chemical Engineering Journal 421 (2021), https://doi.org/10.1016/j.cej.2020.127752.

[2] M. Khodaei, A.M. Gholizadeh, SiC nanoparticles incorporation in electroless NiP-Graphene oxide nanocomposite coatings, Ceramics International 47 (18) (2021) 25287–25295, https://doi.org/10.1016/j.ceramint.2021.05.250.

[3] A. Hassanein, A. Khan, E. Fayyad, A.M. Abdullah, R. Kahraman, B. Mansoor, R. A. Shakoor, Multilevel self-healing characteristics of smart polymeric composite coatings, ACS Applied Materials and Interfaces 13 (43) (2021) 51459–51473, https://doi.org/10.1021/acsami.1c14406.

[4] A. Lelevic, F.C. Walsh, Electrodeposition of Ni[sbnd]P Composite Coatings: A Review. *Surface And Coatings Technology*, Elsevier B.V, 2019, November 25, https://doi.org/10.1016/j.surfcoat.2019.07.027.

[5] J. Sudagar, J. Lian, W. Sha, September 15). Electroless nickel, alloy, composite, and nano coatings - a critical review, Journal of Alloys and Compounds (2013), https://doi.org/10.1016/j.jallcom.2013.03.107.

[6] E.M. Fayyad, A.M. Abdullah, M.K. Hassan, A.M. Mohamed, G. Jarjoura, Z. Farhat, Recent advances in electroless-plated Ni-P and its composites for erosion and corrosion applications: a review, Emergent Materials. Springer Nature (2018, June 1), https://doi.org/10.1007/s42247-018-0010-4.

[7] R.A. Shakoor, R. Kahraman, W. Gao, Y. Wang, Synthesis, characterization, and applications of electroless Ni-B coatings-A review, Int. J. Electrochem. Sci. 11 (2016) 2486–2512. Electrochemical Science Group.

[8] A. Sadeghzadeh-Attar, G. AyubiKia, M. Ehteshamzadeh, Improvement in tribological behavior of novel sol-enhanced electroless Ni-P-SiO2 nanocomposite coatings, Surface and Coatings Technology 307 (2016) 837–848, https://doi.org/10.1016/j.surfcoat.2016.10.026.

[9] R. Hu, Y. Su, Y. Liu, H. Liu, Y. Chen, C. Cao, H. Ni, Deposition process and properties of electroless Ni-P-Al2O3 composite coatings on magnesium alloy, Nanoscale Research Letters 13 (2018), https://doi.org/10.1186/s11671-018-2608-0.

[10] E.M. Fayyad, A.M. Abdullah, A.M.A. Mohamed, G. Jarjoura, Z. Farhat, M. K. Hassan, Effect of electroless bath composition on the mechanical, chemical, and electrochemical properties of new NiP–C3N4 nanocomposite coatings, Surface and Coatings Technology 362 (2019) 239–251, https://doi.org/10.1016/j.surfcoat.2019.01.087.

[11] H. Luo, M. Leitch, H. Zeng, J.L. Luo, Characterization of microstructure and properties of electroless duplex Ni-W-P/Ni-P-nano-ZrO2 composite coating, Materials Today Physics 4 (2018) 36–42, https://doi.org/10.1016/j.mtphys.2018.03.001.

[12] S. Ranganatha, T.V. Venkatesha, Fabrication and anti-corrosion performance of Ni–P–BN nanocomposite coatings on mild steel, Surface Engineering and Applied Electrochemistry 53 (5) (2017) 449–455, https://doi.org/10.3103/S106837551705009X.

[13] V.B. Chintada, R. Koona, Influence of SiC nano-particles on microhardness and corrosion resistance of electroless Ni–P coatings, Journal of Bio- and Tribo-Corrosion 4 (4) (2018), https://doi.org/10.1007/s40735-018-0186-4.

[14] V.K.W. Grips, V. Ezhil Selvi, H.C. Barshilia, K.S. Rajam, Effect of electroless nickel interlayer on the electrochemical behavior of single-layer CrN, TiN, TiAlN coatings, and nanolayered TiAlN/CrN multilayer coatings prepared by reactive dc magnetron sputtering, Electrochimica Acta 51 (17) (2006) 3461–3468, https://doi.org/10.1016/j.electacta.2005.09.042.

[15] H.M. Wu, W.J. Tseng, Electroless nickel metallization to prepare SiO2-Ni composite particles via polyelectrolytes route, Ceramics International 41 (1) (2015) 1863–1868, https://doi.org/10.1016/j.ceramint.2014.09.138.

[16] M. Rezagholizadeh, M. Ghaderi, A. Heidary, S.M.M. Vaghefi, Electroless Ni-P/Ni-B-B4C duplex composite coatings for improving the corrosion and tribological behavior of Ck45 steel, Protection of Metals and Physical Chemistry of Surfaces 51 (2) (2015) 234–239, https://doi.org/10.1134/S207020511502015X.

[17] P.C. Yu, D.Q. Yi, B. Hu, H.Q. Liu, Preparation and microstructure of Ni-coated TiC composite powder by electroless plating, Zhongguo Youse Jinshu Xuebao/Chinese Journal of Nonferrous Metals 23 (2) (2013) 439–447.

[18] H. Luo, M. Leitch, Y. Behnamian, Y. Ma, H. Zeng, J.L. Luo, Development of electroless Ni-P/nano-WC composite coatings and investigation on its properties, Surface and Coatings Technology 277 (2015) 99–106, https://doi.org/10.1016/j.surfcoat.2015.07.011.

[19] M.A. Shoeib, M.M. Kamel, S.M. Rashwan, O.M. Hafez, Corrosion behavior of electroless Ni-P/TiO2 nanocomposite coatings, Surface and Interface Analysis 47 (6) (2015) 672–680, https://doi.org/10.1002/sia.5764.

[20] Y. Wang, S.L. Tay, S. Wei, C. Xiong, W. Gao, R.A. Shakoor, R. Kahraman, Microstructure and properties of sol-enhanced Ni-Co-TiO2 nanocomposite coatings on mild steel, Journal of Alloys and Compounds 649 (2015) 222–228, https://doi.org/10.1016/j.jallcom.2015.07.147.

[21] X. Wu, J. Mao, Z. Zhang, Y. Che, Improving the properties of 211Z Al alloy by enhanced electroless Ni-P-TiO2 nanocomposite coatings with TiO2 sol, Surface and Coatings Technology 270 (2015) 170–174, https://doi.org/10.1016/j.surfcoat.2015.03.006.

[22] S.H. Mousavi Anijdan, M. Sabzi, M.R. Zadeh, M. Farzam, The effect of electroless bath parameters and heat treatment on the properties of Ni-P and Ni-P-Cu composite coatings, Materials Research 21 (2) (2018), https://doi.org/10.1590/1980-5373-MR-2017-0973.

[23] V. Vitry, A. Sens, A.F. Kanta, F. Delaunois, Wear and corrosion resistance of heat-treated and as-plated Duplex NiP/NiB coatings on 2024 aluminum alloys, Surface and Coatings Technology 206 (16) (2012) 3421–3427, https://doi.org/10.1016/j.surfcoat.2012.01.049.

[24] K. Shahzad, E.M. Fayyad, M. Nawaz, O. Fayyaz, R.A. Shakoor, M.K. Hassan, A. M. Abdullah, Corrosion and heat treatment study of electroless nip-ti nanocomposite coatings deposited on hsla steel, Nanomaterials 10 (10) (2020) 1–19, https://doi.org/10.3390/nano10101932.

[25] S. Wang, X. Huang, M. Gong, W. Huang, Microstructure and mechanical properties of Ni-P-Si3N4 nanowire electroless composite coatings, Applied Surface Science 357 (2015) 328–332, https://doi.org/10.1016/j.apsusc.2015.09.011.

[26] X.W. Zhou, Y.F. Shen, H.M. Jin, Study on the preparation and anti-corrosion performance of Ni-P/n-CeO2 composite coatings, Gongneng Cailiao/Journal of Functional Materials 42 (2) (2011) 305–309.

[27] F.C. Walsh, C. Ponce De Leon, A Review of the Electrodeposition of Metal Matrix Composite Coatings by Inclusion of Particles in a Metal Layer: an Established and Diversifying Technology, Transactions of the Institute of Metal Finishing. Maney Publishing, 2014, https://doi.org/10.1179/0020296713Z.000000000161.

[28] C.A. Loto, Electroless nickel plating – a review. *Silicon*, Springer Netherlands, https://doi.org/10.1007/s12633-015-9367-7, 2016, April 1.

[29] L. Ma, Y. Chen, P. Renner, D. Parkinson, A. Fang, H. Liang, Synthesis and morphological characterization of electroless- deposited Ni-P coatings on diamond abrasives, Lubricants 9 (2) (2021) 1–22, https://doi.org/10.3390/lubricants9020020.

[30] Y.L. Wang, X. Xiong, G.D. Li, H.B. Zhang, Z.K. Chen, W. Sun, X.J. Zhao, Microstructure and ablation behavior of hafnium carbide coating for carbon/carbon composites, Surface and Coatings Technology 206 (11–12) (2012) 2825–2832, https://doi.org/10.1016/j.surfcoat.2011.12.001.

[31] H.I. Yoo, H.S. Kim, B.G. Hong, I.C. Sihn, K.H. Lim, B.J. Lim, S.Y. Moon, Hafnium carbide protective layer coatings on carbon/carbon composites deposited with a vacuum plasma spray coating method, Journal of the European Ceramic Society 36 (7) (2016) 1581–1587, https://doi.org/10.1016/j.jeurceramsoc.2016.01.032.

[32] G. Li, G. Li, Microstructure and mechanical properties of hafnium carbide coatings synthesized by reactive magnetron sputtering, Journal of Coatings Technology and Research 7 (3) (2010) 403–407, https://doi.org/10.1007/s11998-009-9225-x.

[33] M. Czagány, P. Baumli, G. Kaptay, The influence of the phosphorous content and heat treatment on the nano-micro-structure, thickness, and micro-hardness of electroless Ni-P coatings on steel, Applied Surface Science 423 (2017) 160–169, https://doi.org/10.1016/j.apsusc.2017.06.168.

[34] J. Wojewoda-Budka, A. Wierzbicka-Miernik, L. Litynska-Dobrzynska, M. J. Szczerba, G. Mordarski, M. Mosiałek, P. Zieba, Microstructure characteristics and phase transformations of the Ni-P and Ni-P-Re electroless deposited coatings after heat treatment, Electrochimica Acta 209 (2016) 183–191, https://doi.org/10.1016/j.electacta.2016.05.043.

[35] B. Li, W. Zhang, Microstructural, surface and electrochemical properties of pulse electrodeposited Ni–W/Si3N4 nanocomposite coating, Ceramics International 44 (16) (2018) 19907–19918, https://doi.org/10.1016/j.ceramint.2018.07.254.

[36] A. Bahgat Radwan, K. Ali, R.A. Shakoor, H. Mohammed, T. Alsalama, R. Kahraman, M. Helal, Properties enhancement of Ni-P electrodeposited coatings by the incorporation of nanoscale Y 2 O 3 particles, Applied Surface Science 457 (2018) 956–967, https://doi.org/10.1016/j.apsusc.2018.06.241.
[37] H. Luo, X. Wang, S. Gao, C. Dong, X. Li, Synthesis of a duplex Ni-P-YSZ/Ni-P nanocomposite coating and investigation of its performance, Surface and Coatings Technology 311 (2017) 70–79, https://doi.org/10.1016/j.surfcoat.2016.12.075.
[38] E.M. Fayyad, M.K. Hassan, K. Rasool, K.A. Mahmoud, A.M.A. Mohamed, G. Jarjoura, A.M. Abdullah, Novel electroless deposited corrosion-resistant and anti-bacterial NiP–TiNi nanocomposite coatings, Surface and Coatings Technology 369 (2019) 323–333, https://doi.org/10.1016/j.surfcoat.2019.04.064.
[39] G.S. Song, S. Sun, Z.C. Wang, C.Z. Luo, C.X. Pan, Synthesis and characterization of electroless Ni-P/Ni-Mo-P duplex coating with different thickness combinations, Acta Metallurgica Sinica (English Letters) 30 (10) (2017) 1008–1016, https://doi.org/10.1007/s40195-017-0603-6.
[40] K. Hans, S. Latha, P. Bera, H.C. Barshilia, Hafnium carbide based solar absorber coatings with high spectral selectivity, Solar Energy Materials and Solar Cells 185 (2018) 1–7, https://doi.org/10.1016/j.solmat.2018.05.005.
[41] T.P. Smirnova, L.V. Yakovkina, V.N. Kitchai, V.V. Kaichev, Y.V. Shubin, N. B. Morozova, K.V. Zherikova, Chemical vapor deposition and characterization of hafnium oxide films, Journal of Physics and Chemistry of Solids 69 (2–3) (2008) 685–687, https://doi.org/10.1016/j.jpcs.2007.07.123.
[42] N. Ohtsu, B. Tsuchiya, M. Oku, T. Shikama, K. Wagatsuma, X-ray photoelectron spectroscopic study on initial oxidation of hafnium hydride fractured in an ultra-high vacuum, Applied Surface Science 253 (16) (2007) 6844–6847, https://doi.org/10.1016/j.apsusc.2007.01.117.
[43] T.L. Barr, S. Seal, Nature of the use of adventitious carbon as a binding energy standard, Journal of Vacuum Science & Technology A: Vacuum, Surfaces, and Films 13 (3) (1995) 1239–1246, https://doi.org/10.1116/1.579868.
[44] D.J. Miller, M.C. Biesinger, N.S. McIntyre, Interactions of CO2 and CO at fractional atmosphere pressures with iron and iron oxide surfaces: one possible mechanism for surface contamination? Surface and Interface Analysis 33 (4) (2002) 299–305, https://doi.org/10.1002/sia.1188.
[45] J. Guillot, A. Jouaiti, L. Imhoff, B. Domenichini, O. Heintz, S. Zerkout, S. Bourgeois, Adventitious carbon growth on aluminium and gold-aluminium alloy surfaces, Surface and Interface Analysis 33 (7) (2002) 591–594, https://doi.org/10.1002/sia.1425.
[46] W. Chen, W. Gao, Y. He, A novel electroless plating of Ni-P-TiO2 nanocomposite coatings, Surface and Coatings Technology 204 (15) (2010) 2493–2498, https://doi.org/10.1016/j.surfcoat.2010.01.032.
[47] A. Stankiewicz, J. Winiarski, M. Stankiewicz, I. Szczygieł, B. Szczygieł, Corrosion resistance evaluation of Ni-P\nano-ZrO2 composite coatings by electrochemical impedance spectroscopy and machine vision method, Materials and Corrosion 66 (7) (2015) 643–648, https://doi.org/10.1002/maco.201407831.
[48] P. Narasimman, M. Pushpavanam, V.M. Periasamy, Synthesis, characterization, and comparison of sediment electro-co-deposited nickel-micro and nano SiC composites, Applied Surface Science 258 (1) (2011) 590–598, https://doi.org/10.1016/j.apsusc.2011.08.038.
[49] J.N. Balaraju, Kalavati, K.S. Rajam, Influence of particle size on the microstructure, hardness, and corrosion resistance of electroless Ni-P-Al2O3 composite coatings, Surface and Coatings Technology 200 (12–13) (2006) 3933–3941, https://doi.org/10.1016/j.surfcoat.2005.03.007.
[50] O. Fayyaz, A. Khan, R.A. Shakoor, A. Hasan, M.M. Yusuf, M.F. Montemor, P. C. Okonkwo, Enhancement of mechanical and corrosion resistance properties of electrodeposited Ni–P–TiC composite coatings, Scientific Reports 11 (1) (2021), https://doi.org/10.1038/s41598-021-84716-6.
[51] A. Hadipour, S.M. Monirvaghefi, M.E. Bahrololoom, Electroless deposition of graded Ni-P coatings, Surface Engineering 31 (6) (2015) 399–405, https://doi.org/10.1179/1743294414Y.0000000430.
[52] M.M. Yusuf, A.B. Radwan, R.A. Shakoor, M. Awais, A.M. Abdullah, M. F. Montemor, R. Kahraman, Synthesis and characterization of Ni–B/Ni–P–CeO2 duplex composite coatings, Journal of Applied Electrochemistry 48 (4) (2018) 391–404, https://doi.org/10.1007/s10800-018-1168-4.
[53] B. Bakhit, A. Akbari, Synthesis and characterization of Ni-Co/SiC nanocomposite coatings using sediment co-deposition technique, Journal of Alloys and Compounds 560 (2013) 92–104, https://doi.org/10.1016/j.jallcom.2013.01.122.
[54] A.P. Meshram, M.K. Punith Kumar, C. Srivastava, Enhancement in the corrosion resistance behaviour of amorphous Ni–P coatings by incorporation of graphene, Diamond and Related Materials 105 (2020), https://doi.org/10.1016/j.diamond.2020.107795.
[55] N. Ghavidel, S.R. Allahkaram, R. Naderi, M. Barzegar, H. Bakhshandeh, Corrosion and wear behavior of an electroless Ni-P/nano-SiC coating on AZ31 Mg alloy obtained through environmentally-friendly conversion coating, Surface and Coatings Technology 382 (2020), https://doi.org/10.1016/j.surfcoat.2019.125156.
[56] M. Sajjadnejad, S.M.S. Haghshenas, V. Tavakoli Targhi, N. Setoudeh, A. Hadipour, A. Moghanian, S. Hosseinpour, Wear behavior of alkaline pulsed electrodeposited nickel composite coatings reinforced by ZnO nanoparticles, Wear 468 (2021) 469, https://doi.org/10.1016/j.wear.2020.203591.
[57] A. Ahmadi Ashtiani, S. Faraji, S. Amjad Iranagh, A.H. Faraji, The study of electroless Ni–P alloys with different complexing agents on Ck45 steel substrate, Arabian Journal of Chemistry 10 (2017) S1541–S1545, https://doi.org/10.1016/j.arabjc.2013.05.015.
[58] M.H. Sliem, K. Shahzad, V.N. Sivaprasad, R.A. Shakoor, A.M. Abdullah, O. Fayyaz, M.A. Umer, Enhanced mechanical and corrosion protection properties of pulse electrodeposited NiP-ZrO2 nanocomposite coatings, Surface and Coatings Technology 403 (2020), https://doi.org/10.1016/j.surfcoat.2020.126340.
[59] W.H. Lee, C.H. Huang, Y.T. Sun, H. Chang, C.Y. Hsu, Tribological properties of Ni-P electroless coatings on low-carbon steel substrates using an environmentally friendly pretreatment, Int. J. Electrochem. Sci. 13 (2) (2018) 2044–2053.
[60] T. Rabizadeh, S.R. Allahkaram, Corrosion resistance enhancement of Ni-P electroless coatings by incorporation of nano-SiO2 particles, Materials and Design 32 (1) (2011) 133–138, https://doi.org/10.1016/j.matdes.2010.06.021.